

NUMERICAL STUDY OF COMPRESSIBLE NAVIER–STOKES–CAHN–HILLIARD SYSTEM*

QIAOLIN HE[†] AND XIAODING SHI[‡]

Abstract. In this paper, we present a relaxation scheme coupled with a stabilized method to numerically study the compressible Navier-Stokes-Cahn-Hilliard system, which has energy-decaying property under certain conditions. Numerical simulations are carried out to verify the stability of the scheme. Numerical results show that the average concentration difference for the two components of the initial state determines the long-time behavior of the diffusive interface for the two-phase flow, which are consistent with theoretical asymptotic stability results established by the authors.

Keywords. relaxation scheme; Navier-Stokes; Cahn-Hilliard; phase transition; large-time behavior.

AMS subject classifications. 76T10; 65D30; 35L65; 65M06.

1. Introduction

The evolution of the binary compressible mixture is one of the fundamental problems in fluid mechanics, for example, the flow of fluids such as foams, solidification processes, fluid-gas interface etc. These kinds of two-phase flows are supposed to be macroscopically immiscible, but local mixing leads to a narrow transition, known as diffusion interfaces. These flows with diffusion interfaces can be described by the coupled system of Navier-Stokes equations and Cahn-Hilliard equations. This mathematical model was first proposed by Lowengrub and Truskinovsky [1], they added the effect of the motion of particles and the interaction with the diffusion into the Cahn-Hilliard equation, and put forward the Navier-Stokes-Cahn-Hilliard system (the so called NSCH model). A similar result was established by Abels and Feireisl [2], Anderson, McFadden and Wheeler [3], Heida, Málek and Rajagopal [4], Kotschote [5] and the references therein. The global existence of renormalized weak solutions of this NSCH system in three dimensions was obtained in Abels and Feireisl [2], the method they used is the framework which was proposed by Lions [6]. Kotschote and Zacher [7] established a local existence of strong solutions in a bounded domain in \mathbb{R}^n . Ding and Li [8] presented the global existence of strong solutions in an interval with no penetration boundary condition in one dimension. Chen, He, Mei and Shi [9] study the asymptotic stability of solutions for this system, they proved that the solutions are asymptotically stable in time even for the large initial disturbance of the density and velocity data. They showed that the average concentration difference for the two components of the initial state determines the long-time behavior of the diffusive interface for the two-phase flow.

We also note that there are many theoretical and numerical results (see [10–15]) on Cahn-Hilliard equation. In [16], the authors presented a gradient stable scheme for incompressible NSCH system with generalized Navier slip boundary condition. The scheme is semi-implicit in time and is based on a convex splitting of the Cahn-Hilliard free energy (including the boundary energy) together with a projection method for the Navier-Stokes equations. The authors of [17] presented a least-squares/finite element method for incompressible NSCH system, which is based on stabilized method for

*Received: January 03, 2019; Accepted (in revised form): November 08, 2019. Communicated by François Bouchut.

[†]School of Mathematics, Sichuan University, Chengdu, 610064, China (qlhejenny@scu.edu.cn).

[‡]Department of Mathematics, School of Science, Beijing University of Chemical Technology, Beijing, 100029, China (shixd@mail.buct.edu.cn).

Cahn-Hilliard equation. In [18], an accurate and energy stable discontinuous Galerkin method has been presented for phase field models of two-phase incompressible flows. There are also other related works about incompressible NSCH system. To the best of our knowledge, for quasi-incompressible and compressible NSCH models, there are few works. The approaches which are used to propose energy-stable schemes for incompressible flows are not applicable to quasi-incompressible and compressible cases, since the pressure is now a function of density and concentration difference.

In this article, we are going to use the relaxation scheme for conservation laws combined with a stabilized method to numerically simulate the coupled NSCH system. The relaxation scheme is introduced by Jin and Xin in [19]. The idea is to use a local relaxation approximation. They construct a linear hyperbolic system with a stiff lower order term that approximates the original system with a small dissipative correction. The main features of this class of schemes is its simplicity and generality. It uses neither Riemann solver spatially nor nonlinear systems of algebraic equation solvers temporally, yet can achieve high-order accuracy and pick up the correct weak solutions. Shen and Yang [20] presented stability analysis and error estimates for a number of commonly used numerical schemes for Allen-Cahn and Cahn-Hilliard equations, which will be used in this article.

The rest of this article is organized as follows. In Section 2, the relaxation schemes for 1-D case and 2-D case are described. In Section 3, we derive the energy law for the PDE system. Discrete energy law of our scheme is derived in Section 4. Numerical tests are performed in Section 5. The paper concludes in Section 6 with a few remarks.

2. The relaxation systems

In this section, first of all, we briefly recall the derivation of the NSCH model, for more details please refer to [1]–[5] and [10]. Let $\Omega \subset \mathbb{R}^N$ be a bounded domain, we define M_i as the mass of the components in the representative material volume V , $\chi_i = \frac{M_i}{M}$ the mass concentration of the fluid, with $i=1,2$, and we introduce the concentration difference of two components for the fluid mixture as $\chi = \chi_1 - \chi_2$. Let $\rho_i = \frac{M_i}{V}$ be the apparent mass density of the fluid i . The total density is defined as $\rho = \rho_1 + \rho_2$. The average velocity u is given by $\rho u = \rho_1 u_1 + \rho_2 u_2$, where u_i is the velocity of the fluid, with $i=1,2$ in the mixed flow. Then the mass conservation equation is obtained immediately

$$\partial_t \rho + \operatorname{div}(\rho u) = 0. \quad (2.1)$$

Let $\epsilon > 0$ be the thickness of the diffuse interface of the fluid mixture, the Helmholtz free energy in the immiscible compressible two-phase fluids is expressed as

$$E_{\text{free}}(\rho, \chi) \stackrel{\text{def}}{=} \int_{\Omega} \left(\frac{\rho^\gamma}{\gamma-1} + \frac{\rho}{\epsilon} f(\chi) + \frac{\epsilon}{2} |\nabla \chi|^2 \right) dx, \quad (2.2)$$

where $\gamma > 1$ is the adiabatic constant, and f represents a “double-well potential”, which is defined as

$$f(\chi) = \frac{1}{4} (\chi^2 - 1)^2. \quad (2.3)$$

We define the free energy density as

$$\Psi(\rho, \chi, \nabla \chi) \stackrel{\text{def}}{=} \frac{\rho^\gamma}{\gamma-1} + \frac{\rho}{\epsilon} f(\chi) + \frac{\epsilon}{2} |\nabla \chi|^2, \quad (2.4)$$

then the non-hydrostatic Cauchy stress tensor P , which is assumed to be of the form

$$P \stackrel{\text{def}}{=} \rho^2 \frac{\partial(\frac{1}{\rho} \Psi)}{\partial \rho} \mathbb{I} + \rho \nabla \chi \otimes \frac{\partial(\frac{1}{\rho} \Psi)}{\partial \nabla \chi} = \rho^\gamma \mathbb{I} - \frac{\epsilon}{2} |\nabla \chi|^2 \mathbb{I} + \epsilon \nabla \chi \otimes \nabla \chi, \quad (2.5)$$

where \mathbb{I} is the unit matrix and ∇ is the gradient operator. Thus the momentum equation reads as

$$\partial_t(\rho u) + \operatorname{div}(\rho u \otimes u) + \nabla p - (\nu \Delta u + \lambda \nabla \operatorname{div} u) = -\epsilon \operatorname{div}(\nabla \chi \otimes \nabla \chi - \frac{|\nabla \chi|^2}{2} \mathbb{I}), \quad (2.6)$$

where div is the divergence operator, $p = \rho^\gamma$ and $\nu > 0$, $\lambda > 0$ are viscosity coefficients. Further, by using the second law of thermodynamics/local dissipation inequality etc., the convected analogue of the Cahn-Hilliard equation can be expressed as

$$\partial_t(\rho \chi) + \operatorname{div}(\rho \chi u) = \Delta \mu. \quad (2.7)$$

Here, μ is the chemical potential, and it can be obtained by the variation of free energy

$$\rho \mu \stackrel{\text{def}}{=} \frac{\delta E_{\text{free}}}{\delta \chi} = \frac{\partial F}{\partial \chi} + \operatorname{div} \frac{\partial F}{\partial \nabla \chi} = \frac{\rho}{\epsilon} \frac{\partial f}{\partial \chi} - \epsilon \Delta \chi. \quad (2.8)$$

So far, combining (2.1), (2.6), (2.7) and (2.8), the compressible Navier-Stokes-Cahn-Hilliard system is derived

$$\begin{aligned} \partial_t \rho + \operatorname{div}(\rho u) &= 0, \\ \partial_t(\rho u) + \operatorname{div}(\rho u \otimes u) + \nabla p - (\nu \Delta u + \lambda \nabla \operatorname{div} u) &= \epsilon \operatorname{div}(\frac{|\nabla \chi|^2}{2} \mathbb{I} - \nabla \chi \otimes \nabla \chi), \\ \partial_t(\rho \chi) + \operatorname{div}(\rho \chi u) &= \Delta \mu, \\ \rho \mu &= \frac{\rho}{\epsilon} \frac{\partial f}{\partial \chi} - \epsilon \Delta \chi. \end{aligned} \quad (2.9)$$

For simplicity, the initial value problem NSCH system in 1-D is

$$\begin{aligned} \rho_t + (\rho u)_x &= 0, \\ \rho u_t + \rho u u_x + p_x &= \nu u_{xx} - \frac{\epsilon}{2} (\chi_x^2)_x, \\ \rho \chi_t + \rho u \chi_x &= \mu_{xx}, \\ \rho \mu &= \frac{1}{\epsilon} \rho \frac{\partial f(\chi)}{\partial \chi} - \epsilon \chi_{xx}, \\ (\rho, u, \chi)(x, 0) &= (\rho_0, u_0, \chi_0)(x). \end{aligned} \quad (2.10)$$

We study two model cases for (2.10): periodic boundary conditions are applied for ρ , u , χ and μ ; another case is that $u|_{\partial\Omega} = 0$, $\frac{\partial \chi}{\partial x}|_{\partial\Omega} = 0$ and $\frac{\partial \mu}{\partial x}|_{\partial\Omega} = 0$. For a complex system, in order to avoid solving a hyperbolic system by Riemann solver and achieving high order accuracy, we approximate the original system with a small dissipative correction, see [21–24]. Letting $\mathbf{u} = (\rho, \rho u)^T$ and $F(\mathbf{u}) = (\rho u, \rho u^2 + p - \nu u_x + \frac{\epsilon}{2} \chi_x^2)^T$, and introducing a new variable $\mathbf{v} \in \mathbb{R}^2$, following from [19], the relaxation system of (2.10) can be introduced

as:

$$\begin{aligned} \frac{\partial}{\partial t}\mathbf{u} + \frac{\partial}{\partial x}\mathbf{v} &= 0 \\ \frac{\partial}{\partial t}\mathbf{v} + A \frac{\partial}{\partial x}\mathbf{u} &= -\frac{1}{\eta}(\mathbf{v} - F(\mathbf{u})), \\ \rho\chi_t + \rho u\chi_x &= \mu_{xx}, \\ \rho\mu &= \frac{1}{\epsilon}\rho \frac{\partial f(\chi)}{\partial \chi} - \epsilon\chi_{xx}, \end{aligned} \quad (2.11)$$

where $\mathbf{u} \in \mathbb{R}^2, \mathbf{v} \in \mathbb{R}^2, x \in \mathbb{R}^1, t > 0$ and $A = \text{diag}(a_1, a_2), a_i > 0 (1 \leq i \leq 2)$. For η sufficiently small, it is expected that by solving (2.11) properly, one can obtain good approximations to the original equations (2.10), where η is a small positive parameter called the relaxation time and A satisfies Liu's subcharacteristic condition

$$A \geq F'(\mathbf{u})^2, \quad \forall \mathbf{u}, \quad (2.12)$$

where $F'(\mathbf{u})$ is the Jacobian matrix of F . Since \mathbf{v} can be eliminated from (2.11), the first two equations in (2.10) can be approximated when $\eta \rightarrow 0$, i.e., small relaxation limit. The viscosity term and a derivative term of χ appearing in the right-hand side of (2.10) will be included in $F(\mathbf{u})$ in (2.11). The relaxation system is a linear system with a stiff lower order term, so we can use efficient splitting time discretizations. One simple choice of the matrix A is

$$a_1 = a_2 = a = \max \left\{ \sup \left(u + \sqrt{p'(\rho)} \right)^2, \sup \left(u - \sqrt{p'(\rho)} \right)^2 \right\}. \quad (2.13)$$

2.1. The relaxation schemes and stabilized method. Similarly as in [19], we define the spatial grid points $x_{j+\frac{1}{2}}$ with mesh size $h_j = x_{j+\frac{1}{2}} - x_{j-\frac{1}{2}}$. We denote by $\mathbf{u}_{j+1/2}$ the approximate point value of \mathbf{u} , and by \mathbf{u}_j the approximate cell average of \mathbf{u} in the cell $[x_{j-1/2}, x_{j+1/2}]$. A spatial discretization to system (2.11)₁₋₂ can be written as

$$\begin{aligned} \frac{\partial}{\partial t}\mathbf{u}_j + \frac{1}{h_j}(\mathbf{v}_{j+1/2} - \mathbf{v}_{j-1/2}) &= 0, \\ \frac{\partial}{\partial t}\mathbf{v}_j + \frac{1}{h_j}A(\mathbf{u}_{j+1/2} - \mathbf{u}_{j-1/2}) &= -\frac{1}{\eta}(\mathbf{v}_j - F_j), \end{aligned} \quad (2.14)$$

where F_j is defined by $F_j = \frac{1}{h_j} \int_{x_{j-1/2}}^{x_{j+1/2}} F(\mathbf{u}) dx = \frac{1}{h_j} F \left(\int_{x_{j-1/2}}^{x_{j+1/2}} \mathbf{u} dx \right) + O(h^2) = F(\mathbf{u}_j) + O(h^2)$, for $h = \max_j h_j$. It is easy to observe that the relaxation system (2.11)₁₋₂ has two characteristic variables $\mathbf{v} \pm A^{\frac{1}{2}}\mathbf{u}$. We shall consider the upwind scheme and the MUSCL scheme, which are described in [19].

The upwind scheme. When we apply the first-order upwind scheme to $\mathbf{v} \pm A^{\frac{1}{2}}\mathbf{u}$, we obtain that

$$\begin{aligned} \mathbf{u}_{j+1/2} &= \frac{1}{2}(\mathbf{u}_j + \mathbf{u}_{j+1}) - \frac{1}{2}A^{-\frac{1}{2}}(\mathbf{v}_{j+1} - \mathbf{v}_j), \\ \mathbf{v}_{j+1/2} &= \frac{1}{2}(\mathbf{v}_j + \mathbf{v}_{j+1}) - \frac{1}{2}A^{\frac{1}{2}}(\mathbf{u}_{j+1} - \mathbf{u}_j). \end{aligned} \quad (2.15)$$

It is easy to obtain the following semi-discrete approximation to relaxation system (2.11)₁₋₂,

$$\begin{aligned} \frac{\partial}{\partial t} \mathbf{u}_j + \frac{1}{2h_j} (\mathbf{v}_{j+1} - \mathbf{v}_{j-1}) - \frac{1}{2h_j} A^{\frac{1}{2}} (\mathbf{u}_{j+1} - 2\mathbf{u}_j + \mathbf{u}_{j-1}) &= 0, \\ \frac{\partial}{\partial t} \mathbf{v}_j + \frac{1}{2h_j} A (\mathbf{u}_{j+1} - \mathbf{u}_{j-1}) - \frac{1}{2h_j} A^{\frac{1}{2}} (\mathbf{v}_{j+1} - 2\mathbf{v}_j + \mathbf{v}_{j-1}) &= -\frac{1}{\eta} (\mathbf{v}_j - F(\mathbf{u}_j)). \end{aligned} \quad (2.16)$$

The MUSCL scheme. Instead of using the piecewise-constant interpolation which yields a first-order approximation, the MUSCL scheme uses the piecewise-linear interpolation, which is a second-order scheme. When the MUSCL scheme is applied to the q -th components of $\mathbf{v} \pm A^{\frac{1}{2}} \mathbf{u}$, it gives that

$$\begin{aligned} u_{j+1/2} &= \frac{1}{2}(u_j + u_{j+1}) - \frac{1}{2\sqrt{a_q}} (v_{j+1} - v_j) + \frac{1}{4\sqrt{a_q}} (h_j \sigma_j^+ + h_{j+1} \sigma_{j+1}^-), \\ v_{j+1/2} &= \frac{1}{2}(v_j + v_{j+1}) - \frac{\sqrt{a_q}}{2} (u_{j+1} - u_j) + \frac{1}{4} (h_j \sigma_j^+ - h_{j+1} \sigma_{j+1}^-). \end{aligned} \quad (2.17)$$

The approximation of the relaxation system (2.11)₁₋₂ is componentwise as

$$\begin{aligned} \frac{\partial}{\partial t} u_j + \frac{1}{2h_j} (v_{j+1} - v_{j-1}) - \frac{\sqrt{a_q}}{2h_j} (u_{j+1} - 2u_j + u_{j-1}) \\ - \frac{1}{4h_j} (h_{j+1} \sigma_{j+1}^- - h_j (\sigma_j^+ + \sigma_{j-1}^-) + h_{j-1} \sigma_{j-1}^+) &= 0, \\ \frac{\partial}{\partial t} v_j + \frac{1}{2h_j} (u_{j+1} - u_{j-1}) - \frac{\sqrt{a_q}}{2h_j} (v_{j+1} - 2v_j + v_{j-1}) \\ + \frac{\sqrt{a_q}}{4h_j} (h_{j+1} \sigma_{j+1}^- + h_j (\sigma_j^+ - \sigma_{j-1}^-) - h_{j-1} \sigma_{j-1}^+) &= -\frac{1}{\eta} (v_j - F^{(q)}(\mathbf{u}_j)), \end{aligned} \quad (2.18)$$

where u and v are the q -th components of \mathbf{u} and \mathbf{v} respectively, a_q is the q -th component of the principal diagonal in A , $F^{(q)}$ is the q -th component of F , σ_j^\pm is the slope of $v \pm \sqrt{a_q} u$ on the j -th cell, defined by Sweby's notation [26],

$$\begin{aligned} \sigma_j^\pm &= \frac{1}{h_j} (v_{j+1} \pm \sqrt{a_q} u_{j+1} - (v_j \pm \sqrt{a_q} u_j)) \phi(\theta_j^\pm), \\ \theta_j^\pm &= \frac{v_j \pm \sqrt{a_q} u_j - (v_{j-1} \pm \sqrt{a_q} u_{j-1})}{v_{j+1} \pm \sqrt{a_q} u_{j+1} - (v_j \pm \sqrt{a_q} u_j)}. \end{aligned} \quad (2.19)$$

The minmod slope $\phi(\theta) = \max(0, \min(1, \theta))$ is used in this article.

The time discretization. We use a second-order TVD Runge-Kutta splitting scheme for (2.11), which is introduced by Jin [25]. The scheme takes implicit stiff steps and explicit convection steps alternatively, which is given by the following

$$\chi_j^* = \chi_j^n, \quad (2.20)$$

$$\mathbf{u}_j^* = \mathbf{u}_j^n, \quad (2.21)$$

$$\mathbf{v}_j^* = \mathbf{v}_j^n + \frac{\Delta t}{\eta} (\mathbf{v}_j^* - F(\mathbf{u}_j^*)) \quad (2.22)$$

$$\mu_j^{(1)} = \frac{1}{\epsilon} \left(S\chi_j^{(1)} - S\chi_j^* + f\chi_j^* \right) - \frac{\epsilon(\chi_{xx}^{(1)})_j}{\rho_j^*}, \quad (2.23)$$

$$\chi_j^{(1)} = \chi_j^* - \Delta t u_j^* \chi_{xj}^{(1)} + \frac{\Delta t (\mu_{xx}^{(1)})_j}{\rho_j^*}, \quad (2.24)$$

$$\mathbf{u}_j^{(1)} = \mathbf{u}_j^* - \frac{\Delta t}{h_j} (\mathbf{v}_{j+1/2}^* - \mathbf{v}_{j-1/2}^*), \quad (2.25)$$

$$\mathbf{v}_j^{(1)} = \mathbf{v}_j^* - \frac{\Delta t}{h_j} A (\mathbf{u}_{j+1/2}^* - \mathbf{u}_{j-1/2}^*). \quad (2.26)$$

The equations (2.20)–(2.26) is the intermediate step of second-order TVD R-K scheme to update χ, \mathbf{u} and \mathbf{v} , where S is the stabilized parameter which is defined in (4.1) for Cahn-Hilliard equation. The idea of keeping the convection terms explicit has great advantages.

$$\chi_j^{**} = \chi_j^{(1)}, \quad (2.27)$$

$$\mathbf{u}_j^{**} = \mathbf{u}_j^{(1)}, \quad (2.28)$$

$$\mathbf{v}_j^{**} = \mathbf{v}_j^{(1)} - \frac{\Delta t}{\eta} (\mathbf{v}_j^{**} - F(\mathbf{u}_j^{**})) - 2 \frac{\Delta t}{\eta} (\mathbf{v}_j^* - F(\mathbf{u}_j^*)) \quad (2.29)$$

$$\mu_j^{(2)} = \frac{1}{\epsilon} \left(S \chi_j^{(2)} - S \chi_j^{**} + f_{\chi j}^{**} \right) - \frac{\epsilon (\chi_{xx}^{(2)})_j}{\rho_j^{**}}, \quad (2.30)$$

$$\chi_j^{(2)} = \chi_j^{**} - \Delta t u_j^{**} \chi_{xj}^{(2)} + \frac{\Delta t (\mu_{xx}^{(2)})_j}{\rho_j^{**}}, \quad (2.31)$$

$$\mathbf{u}_j^{(2)} = \mathbf{u}_j^{**} - \frac{\Delta t}{h_j} (\mathbf{v}_{j+1/2}^{**} - \mathbf{v}_{j-1/2}^{**}), \quad (2.32)$$

$$\mathbf{v}_j^{(2)} = \mathbf{v}_j^{**} - \frac{\Delta t}{h_j} A (\mathbf{u}_{j+1/2}^{**} - \mathbf{u}_{j-1/2}^{**}). \quad (2.33)$$

The equations (2.27)–(2.33) is the second step to update χ, \mathbf{u} and \mathbf{v} in the TVD R-K scheme. Since the source terms are treated implicitly, this time discretization is stable and independent of η , provided that the CFL condition from the convection is satisfied. Finally,

$$\chi_j^{n+1} = \frac{1}{2} (\chi_j^n + \chi_j^{(2)}), \quad (2.34)$$

$$\mathbf{u}_j^{n+1} = \frac{1}{2} (\mathbf{u}_j^n + \mathbf{u}_j^{(2)}), \quad (2.35)$$

$$\mathbf{v}_j^{n+1} = \frac{1}{2} (\mathbf{v}_j^n + \mathbf{v}_j^{(2)}), \quad (2.36)$$

where $\mathbf{u}_{j+\frac{1}{2}}$ and $\mathbf{v}_{j+\frac{1}{2}}$ can be taken as upwind scheme (2.15) or MUSCL scheme (2.17). In (2.23)–(2.24) and (2.30)–(2.31), we have used a first-order stabilized semi-implicit method for Cahn-Hilliard equation introduced by Shen and Yang in [20]. Actually, a second-order stabilized semi-implicit method for Cahn-Hilliard equation in [20] can still be applied to (2.23)–(2.24) and (2.30)–(2.31) like the following

$$\begin{aligned} -\epsilon \frac{\chi_{xx}^{n+1}}{\rho^n} + S \frac{\chi^{n+1} - 2\chi^n + \chi^{n-1}}{\epsilon} - \mu^{n+1} &= \frac{f_\chi^{n-1} - 2f_\chi^n}{\epsilon} \\ \frac{1}{2\Delta t} (3\chi^{n+1} - 4\chi^n + \chi^{n-1}) &= \frac{\mu_{xx}^{n+1}}{\rho^n} - u^n \chi_x^{n+1} \end{aligned} \quad (2.37)$$

where $S \geq \frac{L}{2}$ and $\max_{\chi} \{|f_{\chi\chi}| \} \leq L$. From (2.22), the algorithm will break down if $\Delta t = O(\eta)$. Therefore, we choose $\Delta t \neq O(\eta)$.

2.2. Two dimensional case. Refer to the Navier-Stokes-Cahn-Hilliard system (2.9), the initial value problem NSCH system in two dimensions can be reduced to

$$\begin{aligned}
 & \rho_t + (\rho u)_x + (\rho v)_y = 0, \\
 & (\rho u)_t + (\rho u^2 + p)_x + (\rho u v)_y \\
 &= \nu \frac{\partial u_x}{\partial x} + \nu \frac{\partial(u_y + v_x)}{\partial y} + \lambda \frac{\partial(u_x + v_y)}{\partial x} - \epsilon \frac{\partial(\frac{1}{2}\chi_x^2 - \frac{1}{2}\chi_y^2)}{\partial x} - \epsilon \frac{\partial(\chi_x \chi_y)}{\partial y}, \\
 & (\rho v)_t + (\rho u v)_x + (\rho v^2 + p)_y \\
 &= \nu \frac{\partial(u_y + v_x)}{\partial x} + \nu \frac{\partial v_y}{\partial y} + \lambda \frac{\partial(u_x + v_y)}{\partial y} - \epsilon \frac{\partial(\chi_x \chi_y)}{\partial x} - \epsilon \frac{\partial(\frac{1}{2}\chi_y^2 - \frac{1}{2}\chi_x^2)}{\partial y}, \\
 & (\rho \chi)_t + \frac{\partial(\rho \chi u)}{\partial x} + \frac{\partial(\rho \chi v)}{\partial y} = \Delta \mu, \\
 & \rho \mu = \frac{1}{\epsilon} \rho \frac{\partial f(\rho, \chi)}{\partial \chi} - \epsilon \operatorname{div}(\nabla \chi), \\
 & (\rho, u, v, \chi)(x, y, 0) = (\rho_0, u_0, v_0, \chi_0)(x, y),
 \end{aligned} \tag{2.38}$$

where λ is also a viscosity coefficient, u represents horizontal velocity and v represents vertical velocity. As in [19], consider the two dimensional relaxation system in Eulerian coordinates,

$$\begin{aligned}
 & \frac{\partial}{\partial t} \mathbf{u} + \frac{\partial}{\partial x} \mathbf{v} + \frac{\partial}{\partial y} \mathbf{w} = 0, \\
 & \frac{\partial}{\partial t} \mathbf{v} + A \frac{\partial}{\partial x} \mathbf{u} = -\frac{1}{\eta} (\mathbf{v} - F(\mathbf{u})), \\
 & \frac{\partial}{\partial t} \mathbf{w} + B \frac{\partial}{\partial y} \mathbf{u} = -\frac{1}{\eta} (\mathbf{w} - G(\mathbf{u})),
 \end{aligned} \tag{2.39}$$

where $A = \operatorname{diag}(a_1, a_2, a_3)$ and $B = \operatorname{diag}(b_1, b_2, b_3)$ with $a_i > 0, b_i > 0$ for $1 \leq i \leq 3$. In two dimensions, $\mathbf{u} = (\rho, \rho u, \rho v)^T$ and

$$\begin{aligned}
 F(\mathbf{u}) &= (\rho u, \rho u^2 + p - 2\nu u_x - \lambda(u_x + v_y) + \frac{1}{2}\epsilon\chi_x^2 - \frac{1}{2}\epsilon\chi_y^2, \rho u v - \nu(u_y + v_x) + \epsilon\chi_x \chi_y)^T, \\
 G(\mathbf{u}) &= (\rho v, \rho u v - \nu(u_y + v_x) + \epsilon\chi_x \chi_y, \rho v^2 + p - 2\nu v_y - \lambda(u_x + v_y) - \frac{1}{2}\epsilon\chi_x^2 + \frac{1}{2}\epsilon\chi_y^2),
 \end{aligned}$$

and $p = \rho^\gamma$ is the pressure. Similar as (2.13), the simple choice for matrix A is

$$a_1 = a_2 = a_3 = a = \max \left\{ \sup \left(u + \sqrt{p'(\rho)} \right)^2, \sup u^2, \sup \left(u - \sqrt{p'(\rho)} \right)^2 \right\}, \tag{2.40}$$

for matrix B is

$$b_1 = b_2 = b_3 = b = \max \left\{ \sup \left(v + \sqrt{p'(\rho)} \right)^2, \sup v^2, \sup \left(v - \sqrt{p'(\rho)} \right)^2 \right\}, \tag{2.41}$$

which corresponds to the eigenvalues of 2-D Euler equations. Suppose the spatial grid points are located at $(x_{i+1/2}, y_{j+1/2})$, the mesh size is $h_i^x = x_{i+1/2} - x_{i-1/2}$ and $h_j^y = y_{j+1/2} - y_{j-1/2}$. For $\mathbf{u}(x, y)$, the point value $\mathbf{u}_{i+1/2, j+1/2} = \mathbf{u}(x_{i+1/2}, y_{j+1/2})$ and the cell average value is defined as

$$\mathbf{u}_{i,j} = \frac{1}{h_i^x h_j^y} \int_{x_{i-1/2}}^{x_{i+1/2}} \int_{y_{j-1/2}}^{y_{j+1/2}} \mathbf{u}(x, y) dx dy. \quad (2.42)$$

A semi-discrete differencing scheme to (2.39) is

$$\begin{aligned} \frac{\partial}{\partial t} \mathbf{u}_{i,j} + \frac{1}{h_i^x} (\mathbf{v}_{i+1/2,j} - \mathbf{v}_{i-1/2,j}) + \frac{1}{h_j^y} (\mathbf{w}_{i,j+1/2} - \mathbf{w}_{i,j-1/2}) &= 0, \\ \frac{\partial}{\partial t} \mathbf{v}_{i,j} + A \frac{1}{h_i^x} (\mathbf{u}_{i+1/2,j} - \mathbf{u}_{i-1/2,j}) &= -\frac{1}{\eta} (\mathbf{v}_{i,j} - F(\mathbf{u}_{i,j})), \\ \frac{\partial}{\partial t} \mathbf{w}_{i,j} + B \frac{1}{h_j^y} (\mathbf{u}_{i,j+1/2} - \mathbf{u}_{i,j-1/2}) &= -\frac{1}{\eta} (\mathbf{w}_{i,j} - G(\mathbf{u}_{i,j})). \end{aligned} \quad (2.43)$$

The similar upwind scheme and MUSCL scheme which are described in [19] can be used in (2.43). For the time discretization, we use the algorithm (2.20)–(2.36), which is second-order in time. The second-order stabilized method (2.37) can be applied in the two dimensional case.

3. Energy law for the system

In this section, we will give the energy equation of system (2.9). We define

$$G(\rho) \stackrel{\text{def}}{=} \rho \int_{\bar{\rho}}^{\rho} \frac{p(s) - p(\bar{\rho})}{s^2} ds. \quad (3.1)$$

where $\bar{\rho} = \frac{1}{|\Omega|} \int_{\Omega} \rho_0(x) dx$ is the average of the initial density. Observing that

$$G'(\rho) = \frac{G(\rho) + p(\rho) - p(\bar{\rho})}{\rho}, \quad \text{and} \quad G''(\rho) = \frac{p'(\rho)}{\rho},$$

one has $G(\bar{\rho}) = G'(\bar{\rho}) = 0$, and then, combining with the convexity property of p , there exist positive constants $c_1, c_2 > 0$ satisfying

$$c_1(\rho - \bar{\rho})^2 \leq G(\rho) \leq c_2(\rho - \bar{\rho})^2. \quad (3.2)$$

Combining with the mass conservation equation (2.9)₁, so that

$$G(\rho)_t + \operatorname{div}(G(\rho)u) + (p(\rho) - p(\bar{\rho})) \operatorname{div} u = 0. \quad (3.3)$$

LEMMA 3.1. *Assume that the initial value $(\rho_0, u_0) \in H^3$ and $\chi_0 \in H^4$, then $\forall T > 0$, it holds that*

$$\begin{aligned} &\sup_{t \in [0, T]} \int_{\Omega} \left(\frac{\rho u^2}{2} + \frac{\epsilon}{2} |\nabla \chi|^2 + c_1 |\rho - \bar{\rho}|^2 + \frac{\rho(\chi^2 - 1)^2}{4\epsilon} \right) dx \\ &\quad + \int_0^T \int_{\Omega} \left(|\nabla \mu|^2 + \nu |\nabla u|^2 + \lambda |\operatorname{div} u|^2 \right) dx dt \\ &\leq \int_{\Omega} \left(\frac{1}{2} \rho_0 u_0^2 + \frac{\epsilon}{2} |\nabla \chi_0|^2 + c_2 |\rho - \bar{\rho}|^2 + \frac{\rho}{4\epsilon} (\chi_0^2 - 1)^2 \right) dx, \end{aligned} \quad (3.4)$$

where C is a positive constant.

Proof. Multiplying Equation (2.9)₂ by u and Equation (2.9)₃ by μ , integrating over Ω and adding them up, one has

$$\frac{d}{dt} \int_{\Omega} \left(\frac{\rho u^2}{2} + \frac{\epsilon}{2} |\nabla \chi|^2 + \frac{\rho(\chi^2 - 1)^2}{4\epsilon} \right) dx + \int_{\Omega} \left(|\nabla \mu|^2 + \nu |\nabla u|^2 + \lambda |\operatorname{div} u|^2 + u \nabla p(\rho) \right) dx = 0.$$

Integrating (3.3) and adding the result to the above equation, one then gets

$$\frac{d}{dt} \int_{\Omega} \left(\frac{\rho u^2}{2} + \frac{\epsilon}{2} |\nabla \chi|^2 + G(\rho) + \frac{\rho(\chi^2 - 1)^2}{4\epsilon} \right) dx + \int_{\Omega} \left(|\nabla \mu|^2 + \nu |\nabla u|^2 + \lambda |\operatorname{div} u|^2 \right) dx = 0,$$

integrating the above equation over $[0, T]$, one has

$$\begin{aligned} & \sup_{t \in [0, T]} \int_{\Omega} \left(\frac{\rho u^2}{2} + \frac{\epsilon}{2} |\nabla \chi|^2 + G(\rho) + \frac{\rho(\chi^2 - 1)^2}{4\epsilon} \right) dx \\ & \quad + \int_0^T \int_{\Omega} \left(|\nabla \mu|^2 + \nu |\nabla u|^2 + \lambda |\operatorname{div} u|^2 \right) dx dt \\ & \leq \int_{\Omega} \left(\frac{1}{2} \rho_0 u_0^2 + \frac{\epsilon}{2} |\nabla \chi_0|^2 + G(\rho_0) + \frac{\rho}{4\epsilon} (\chi_0^2 - 1)^2 \right) dx, \end{aligned} \quad (3.5)$$

combining with the inequality (3.2), the standard energy estimate (3.4) is obtained. \square

4. Discrete energy law

4.1. The Cahn-Hilliard equation. In this section, we will discuss the discrete energy-decaying property for (2.11). To illustrate the procedure, we consider the pure Cahn-Hilliard equation. For the first-order semi-implicit method

$$-\epsilon \frac{(\chi_x^{n+1})_x}{\rho^n} + S \frac{\chi^{n+1}}{\epsilon} - \mu^{n+1} = \frac{S \chi^n - f_\chi^n}{\epsilon}, \quad (4.1)$$

$$\chi^{n+1} - \Delta t \frac{\mu_{xx}^{n+1}}{\rho^n} = \chi^n, \quad (4.2)$$

similar as Lemma 3.2 in [20], we have the following

LEMMA 4.1. For $S \geq \frac{L}{2}$ and $\max_{\chi} \{|f_{\chi\chi}| \} \leq L$, the scheme (4.1)–(4.2) is unconditionally stable and the following energy law holds for any Δt :

$$\int_{\Omega} \left(\frac{\epsilon}{2} (\chi_x^{n+1})^2 + \frac{1}{\epsilon} \rho^n f(\chi^{n+1}) \right) dx \leq \int_{\Omega} \left(\frac{\epsilon}{2} (\chi_x^n)^2 + \frac{1}{\epsilon} \rho^n f(\chi^n) \right) dx. \quad (4.3)$$

REMARK 4.1. The linear version of the second-order scheme (2.37) is conditionally stable for all $S \geq 0$, which is the same as Lemma 2.3. in [20].

4.2. Discrete energy law for the relaxation scheme (2.11). We now present the discrete energy law for the total energy. This also implies the stability of the time discretization scheme (2.20)–(2.36). For simplicity, we consider the first-order TVD Runge-Kutta scheme and use a uniform grid, $h_j = h$.

$$\chi_j^* = \chi_j^n, \quad (4.4)$$

$$\mathbf{u}_j^* = \mathbf{u}_j^n, \quad (4.5)$$

$$\mathbf{v}_j^* = \mathbf{v}_j^n - \frac{\Delta t}{\eta} (\mathbf{v}_j^* - F(\mathbf{u}_j^*)), \quad (4.6)$$

$$\mu_j^{n+1} = \frac{1}{\epsilon} \left(S\chi_j^{n+1} - S\chi_j^* + f_{\chi j}^* \right) - \epsilon \frac{\chi_{j+1}^{n+1} - 2\chi_j^{n+1} + \chi_{j-1}^{n+1}}{h^2 \rho_j^*}, \quad (4.7)$$

$$\chi_j^{n+1} = \chi_j^* - \Delta t u_j^* \frac{\chi_{j+1}^{n+1} - \chi_{j-1}^{n+1}}{2h} + \Delta t \frac{\mu_{j+1}^{n+1} - 2\mu_j^{n+1} + \mu_{j-1}^{n+1}}{h^2 \rho_j^*}, \quad (4.8)$$

$$\mathbf{u}_j^{n+1} = \mathbf{u}_j^* - \frac{\Delta t}{h} (\mathbf{v}_{j+1/2}^* - \mathbf{v}_{j-1/2}^*), \quad (4.9)$$

$$\mathbf{v}_j^{n+1} = \mathbf{v}_j^* - \frac{\Delta t}{h} A (\mathbf{u}_{j+1/2}^* - \mathbf{u}_{j-1/2}^*), \quad (4.10)$$

where $A = \text{diag}(a, a)$ which satisfies Liu's subcharacteristic condition, $\mathbf{u}_{j+1/2}$ and $\mathbf{v}_{j+1/2}$ can be calculated by the upwind scheme (2.15), therefore equations (4.9)–(4.10) can be rewritten as

$$\mathbf{u}_j^{n+1} = \mathbf{u}_j^* - \frac{1}{2} k (\mathbf{v}_{j+1}^* - \mathbf{v}_{j-1}^*) + \frac{1}{2} k \sqrt{a} (\delta_x^2 \mathbf{u}_j^*), \quad (4.11)$$

$$\mathbf{v}_j^{n+1} = \mathbf{v}_j^* - \frac{1}{2} k (\mathbf{u}_{j+1}^* - \mathbf{u}_{j-1}^*) + \frac{1}{2} k \sqrt{a} (\delta_x^2 \mathbf{v}_j^*), \quad (4.12)$$

where $k = \frac{\Delta t}{h}$, $\delta_x^2 \mathbf{u}_j := \mathbf{u}_{j+1} - 2\mathbf{u}_j + \mathbf{u}_{j-1}$, and \mathbf{v}_j^* can be solved in (4.6),

$$\mathbf{v}_j^* = \frac{1}{1 + \frac{\Delta t}{\eta}} \left(\mathbf{v}_j^n + \frac{\Delta t}{\eta} F(\mathbf{u}_j^n) \right). \quad (4.13)$$

We define the discrete l_2 inner product of two real vectors U and V when total cell numbers is J , as follows:

$$\langle U, V \rangle = h \sum_{j=1}^J U_j V_j, \quad (4.14)$$

for which we have $\|U\| = \langle U, U \rangle^{1/2}$.

THEOREM 4.1. *Let $\mathbf{u}^n, \mathbf{v}^n, \chi^n, \mu^n$ satisfy equations (4.4)–(4.10) with periodic boundary conditions for $\mathbf{u}^n, \mathbf{v}^n, \chi^n$ and μ^n . For $S \geq \frac{L}{2}$ and $\max_{\chi} \{|f_{\chi\chi}| \} \leq L$, and if $\frac{\Delta t}{h} \sqrt{a} \leq 1$, we have*

$$\|\sqrt{a} \mathbf{u}^{n+1}\|^2 + \|\mathbf{v}^{n+1}\|^2 \leq \|\sqrt{a} \mathbf{u}^n\|^2 + \|\mathbf{v}^*\|^2. \quad (4.15)$$

Moreover, if at $t=t^n$, the solution is in local equilibrium, i.e.,

$$\mathbf{v}_j^* = \mathbf{v}_j^n, \quad (4.16)$$

we have

$$\begin{aligned} & \|\sqrt{a} \mathbf{u}^{n+1}\|^2 + \|\mathbf{v}^{n+1}\|^2 + \frac{\epsilon}{2h^2} \sum_{j=1}^J (\chi_j^{n+1} - \chi_{j-1}^{n+1})^2 + \frac{1}{\epsilon} \sum_{j=1}^J \rho_j^{n+1} f_j^{n+1} \\ & \leq \|\sqrt{a} \mathbf{u}^n\|^2 + \|\mathbf{v}^n\|^2 + \frac{\epsilon}{2h^2} \sum_{j=1}^J (\chi_j^n - \chi_{j-1}^n)^2 + \frac{1}{\epsilon} \sum_{j=1}^J \rho_j^n f_j^n. \end{aligned} \quad (4.17)$$

Proof. From (4.11) and (4.12), using (4.14), we have

$$\begin{aligned}\|\mathbf{u}^{n+1}\|^2 &= \|\mathbf{u}^*\|^2 + k^2 \|\Delta_{0x} \mathbf{v}^*\|^2 + \frac{k^2}{4} a \|\delta_x^2 \mathbf{u}^*\|^2 \\ &\quad - k \langle \mathbf{u}^*, 2\Delta_{0x} \mathbf{v}^* \rangle + k\sqrt{a} \langle \mathbf{u}^*, \delta_x^2 \mathbf{u}^* \rangle - k^2 \sqrt{a} \langle \Delta_{0x} \mathbf{v}^*, \delta_x^2 \mathbf{u}^* \rangle,\end{aligned}\quad (4.18)$$

$$\begin{aligned}\|\mathbf{v}^{n+1}\|^2 &= \|\mathbf{v}^*\|^2 + k^2 a^2 \|\Delta_{0x} \mathbf{u}^*\|^2 + \frac{k^2}{4} a \|\delta_x^2 \mathbf{v}^*\|^2 \\ &\quad - ka \langle \mathbf{v}^*, 2\Delta_{0x} \mathbf{u}^* \rangle + k\sqrt{a} \langle \mathbf{v}^*, \delta_x^2 \mathbf{v}^* \rangle - k^2 a^{\frac{3}{2}} \langle \Delta_{0x} \mathbf{u}^*, \delta_x^2 \mathbf{v}^* \rangle.\end{aligned}\quad (4.19)$$

where $\Delta_{0x} \mathbf{u}_j := \frac{1}{2}(\mathbf{u}_{j+1} - \mathbf{u}_{j-1})$. Using a times (4.18) and adding to (4.19), we obtain that

$$\begin{aligned}\|\sqrt{a} \mathbf{u}^{n+1}\|^2 + \|\mathbf{v}^{n+1}\|^2 &= \|\sqrt{a} \mathbf{u}^*\|^2 + \|\mathbf{v}^*\|^2 + k^2 a \|\Delta_{0x} \mathbf{v}^*\|^2 \\ &\quad + k^2 a^2 \|\Delta_{0x} \mathbf{u}^*\|^2 + \frac{k^2}{4} a^2 \|\delta_x^2 \mathbf{u}^*\|^2 + \frac{k^2}{4} a \|\delta_x^2 \mathbf{v}^*\|^2 \\ &\quad - ka^{\frac{3}{2}} \|\delta_x \mathbf{u}^*\|^2 - k\sqrt{a} \|\delta_x \mathbf{v}^*\|^2,\end{aligned}\quad (4.20)$$

where $\delta_x \mathbf{u}_j := \mathbf{u}_{j+\frac{1}{2}} - \mathbf{u}_{j-\frac{1}{2}}$, we have used periodic boundary conditions and the summation by parts formulae. The above equation can be rewritten as

$$\begin{aligned}\|\sqrt{a} \mathbf{u}^{n+1}\|^2 + \|\mathbf{v}^{n+1}\|^2 &\leq \|\sqrt{a} \mathbf{u}^*\|^2 + \|\mathbf{v}^*\|^2 \\ &\quad + \frac{k^2}{2} a \|\Delta_{+x} \mathbf{v}^*\|^2 + \frac{k^2}{2} a \|\Delta_{-x} \mathbf{v}^*\|^2 - k\sqrt{a} \|\delta_x \mathbf{v}^*\|^2 \\ &\quad + \frac{k^2}{2} a^2 \|\Delta_{+x} \mathbf{u}^*\|^2 + \frac{k^2}{2} a^2 \|\Delta_{-x} \mathbf{u}^*\|^2 - ka^{\frac{3}{2}} \|\delta_x \mathbf{u}^*\|^2,\end{aligned}\quad (4.21)$$

where $\Delta_{+x} \mathbf{u}_j := \mathbf{u}_{j+1} - \mathbf{u}_j$ and $\Delta_{-x} \mathbf{u}_j := \mathbf{u}_j - \mathbf{u}_{j-1}$. If $k\sqrt{a} \leq 1$, we obtain

$$\|\sqrt{a} \mathbf{u}^{n+1}\|^2 + \|\mathbf{v}^{n+1}\|^2 \leq \|\sqrt{a} \mathbf{u}^n\|^2 + \|\mathbf{v}^n\|^2, \quad (4.22)$$

where $\mathbf{u}^* = \mathbf{u}^n$ has been used, \mathbf{v}^* is composed of $\mathbf{u}^n, \mathbf{v}^n$ and χ^n . If at $t = t^n$, the solution is in local equilibrium, by (4.16), we have

$$\|\sqrt{a} \mathbf{u}^{n+1}\|^2 + \|\mathbf{v}^{n+1}\|^2 \leq \|\sqrt{a} \mathbf{u}^n\|^2 + \|\mathbf{v}^n\|^2. \quad (4.23)$$

Using μ_j^{n+1} times (4.8) and summing up over all j , using $\chi_j^{n+1} - \chi_j^n$ times (4.7) and summing up over all j , we have

$$\begin{aligned}\frac{1}{\epsilon} S \sum_{j=1}^J \rho_j^n (\chi_j^{n+1} - \chi_j^n)^2 &- \frac{\epsilon}{h^2} \sum_{j=1}^J (\chi_{j+1}^{n+1} - 2\chi_j^{n+1} + \chi_{j-1}^{n+1})(\chi_j^{n+1} - \chi_j^n) \\ &\quad + \frac{1}{\epsilon} \sum_{j=1}^J \rho_j^n f_{\chi j}^n (\chi_j^{n+1} - \chi_j^n) = \sum_{j=1}^J \rho_j^n \mu_j^{n+1} (\chi_j^{n+1} - \chi_j^n),\end{aligned}\quad (4.24)$$

$$\begin{aligned}\sum_{j=1}^J \rho_j^n \mu_j^{n+1} (\chi_j^{n+1} - \chi_j^n) &= \frac{\Delta t}{h^2} \sum_{j=1}^J (\mu_{j+1}^{n+1} - 2\mu_j^{n+1} + \mu_{j-1}^{n+1}) \mu_j^{n+1} \\ &\quad - \frac{\Delta t}{2h} \sum_{j=1}^J \rho_j^n u_j^n (\chi_{j+1}^{n+1} - \chi_{j-1}^{n+1}) \mu_j^{n+1},\end{aligned}\quad (4.25)$$

where we have used that $\rho_j^* = \rho_j^n$. Adding (4.24) and (4.25) together and using (4.7) and periodic boundary conditions, we obtain

$$\begin{aligned} & \frac{1}{\epsilon} S \sum_{j=1}^J \rho_j^n (\chi_j^{n+1} - \chi_j^n)^2 + \frac{\epsilon}{2h^2} \sum_{j=1}^J ((\chi_j^{n+1} - \chi_{j-1}^{n+1})^2 - (\chi_j^n - \chi_{j-1}^n)^2 \\ & + ((\chi_j^{n+1} - \chi_{j-1}^{n+1}) - (\chi_j^n - \chi_{j-1}^n))^2) + \frac{1}{\epsilon} \sum_{j=1}^J \rho_j^n f_{\chi j}^n (\chi_j^{n+1} - \chi_j^n) \\ = & - \frac{\Delta t}{h^2} \sum_{j=1}^J (\mu_j^{n+1} - \mu_{j-1}^{n+1})^2 \\ & - \frac{\Delta t}{2h} \sum_{j=1}^J u_j^n (\chi_{j+1}^{n+1} - \chi_{j-1}^{n+1}) \left(\frac{S}{\epsilon} \rho_j^n (\chi_j^{n+1} - \chi_j^n) + \rho_j^n \frac{f_{\chi j}^n}{\epsilon} - \epsilon \frac{\chi_{j+1}^{n+1} - 2\chi_j^{n+1} + \chi_{j-1}^{n+1}}{h^2} \right), \end{aligned}$$

therefore, we arrive at

$$\begin{aligned} & \frac{1}{\epsilon} S \sum_{j=1}^J \rho_j^n (\chi_j^{n+1} - \chi_j^n)^2 + \frac{\epsilon}{2h^2} \sum_{j=1}^J ((\chi_j^{n+1} - \chi_{j-1}^{n+1})^2 - (\chi_j^n - \chi_{j-1}^n)^2 \\ & + ((\chi_j^{n+1} - \chi_{j-1}^{n+1}) - (\chi_j^n - \chi_{j-1}^n))^2) + \frac{1}{\epsilon} \sum_{j=1}^J \rho_j^n f_{\chi j}^n (\chi_j^{n+1} - \chi_j^n) \\ \leq & - \frac{\Delta t}{2h} \sum_{j=1}^J u_j^n (\chi_{j+1}^{n+1} - \chi_{j-1}^{n+1}) \left(\frac{S}{\epsilon} \rho_j^n (\chi_j^{n+1} - \chi_j^n) + \rho_j^n \frac{f_{\chi j}^n}{\epsilon} - \epsilon \frac{\chi_{j+1}^{n+1} - 2\chi_j^{n+1} + \chi_{j-1}^{n+1}}{h^2} \right). \end{aligned} \quad (4.26)$$

Multiplying the first equation of (4.11) by f_j^{n+1} and taking summation over j , we have

$$\begin{aligned} \sum_{j=1}^J \rho_j^{n+1} f_j^{n+1} = & \sum_{j=1}^J \rho_j^n f_j^{n+1} + \frac{k}{2} \sum_{j=1}^J \rho_j^n u_j^n (f_{j+1}^{n+1} - f_{j-1}^{n+1}) \\ & + \frac{\sqrt{ak}}{2} \sum_{j=1}^J \rho_j^n (f_{j+1}^{n+1} - 2f_j^{n+1} + f_{j-1}^{n+1}), \end{aligned} \quad (4.27)$$

where periodic boundary conditions and the summation by parts formulae are used.

Using (4.27) and Taylor expansion, with $S \geq \frac{\max_x \{|f_{\chi\chi}| \}}{2}$, the sum of the terms in (4.26) related to $\frac{1}{\epsilon}$ can be reduced to $\frac{1}{\epsilon} \sum_{j=1}^J (\rho_j^{n+1} f_j^{n+1} - \rho_j^n f_j^n)$. Then the following formulation can be obtained

$$\frac{\epsilon}{2h^2} \sum_{j=1}^J (\chi_j^{n+1} - \chi_{j-1}^{n+1})^2 - \frac{\epsilon}{2h^2} \sum_{j=1}^J (\chi_j^n - \chi_{j-1}^n)^2 + \frac{1}{\epsilon} \sum_{j=1}^J (\rho_j^{n+1} f_j^{n+1} - \rho_j^n f_j^n) \leq 0. \quad (4.28)$$

Combine (4.28) and (4.23), since $\frac{\Delta t}{h} \sqrt{a} \leq 1$, we obtain that

$$\|\sqrt{a}\mathbf{u}^{n+1}\|^2 + \|\mathbf{v}^{n+1}\|^2 + \frac{\epsilon}{2h^2} \sum_{j=1}^J (\chi_j^{n+1} - \chi_{j-1}^{n+1})^2 + \frac{1}{\epsilon} \sum_{j=1}^J \rho_j^{n+1} f_j^{n+1}$$

$$\leq \|\sqrt{a}\mathbf{u}^n\|^2 + \|\mathbf{v}^n\|^2 + \frac{\epsilon}{2h^2} \sum_{j=1}^J (\chi_j^n - \chi_{j-1}^n)^2 + \frac{1}{\epsilon} \sum_{j=1}^J \rho_j^n f_j^n. \quad (4.29)$$

□

REMARK 4.2. The singular limit of the solution for Jin-Xin relaxation system (2.11) as $\eta \rightarrow 0^+$ is an open and important problem. Formally, the relaxation system (2.11) can be approximated to leading order by (2.10) as $\eta \rightarrow 0^+$. In Lemma 3.1, we have shown the energy law for NSCH system (2.9). Since the upper and lower bound estimates of density ρ have been proved in reference [9], the energy in discrete level in Theorem 4.1 is matched with energy in continuous level in Lemma 3.1 up to an error of $O(\frac{\eta}{\Delta t})$. Thus, we have the stability of method (4.4)–(4.10). Although we only present the stability proof when applying the upwind scheme (2.16), numerical results in Section 5 show that when applying MUSCL scheme, stability still holds. Though we only show the stability for first-order TVD Runge-Kutta scheme, it is not difficult to generalize the results to second-order TVD Runge-Kutta scheme (2.20)–(2.36).

5. Numerical results

In this section, we present several numerical examples to study the large-time behavior of solutions to the initial value problems. We use the above second-order TVD Runge-Kutta scheme (2.20)–(2.36), where MUSCL scheme is used in space. The parameters that we choose for example (1) – example (4) in one dimensional cases are

$$\epsilon = 10^{-3}, \quad \eta = 10^{-3}, \quad \nu = 1.0, \quad \gamma = 1.5 \quad (\gamma \geq 1). \quad (5.1)$$

According to Lemma 4.1 and Theorem 4.1, the stability parameter S is taken to be 1.5, both 1-D and 2-D numerical results are given. We will numerically verify the discrete energy law of our scheme which is proved in Theorem 4.1, which is defined as

$$Eng_{1D} = \|\sqrt{a}\mathbf{u}^n\|^2 + \|\mathbf{v}^n\|^2 + \frac{\epsilon}{2h^2} \sum_{j=1}^J (\chi_j^n - \chi_{j-1}^n)^2 + \frac{1}{\epsilon} \sum_{j=1}^J \rho_j^n f_j^n. \quad (5.2)$$

We will also show that the average concentration difference for the two components of the initial state determines the long-time behavior of the diffusive interface for the two-phase flow. This leads to a separation of two regions for the initial concentration difference: regions A_{stable} and A_{unstable} , which correspond to the stable region and unstable region.

$$A_{\text{stable}} = \left(-\infty, -\frac{\sqrt{3}}{3}\right) \cup \left(\frac{\sqrt{3}}{3}, +\infty\right), \quad A_{\text{unstable}} = \left(-\frac{\sqrt{3}}{3}, \frac{\sqrt{3}}{3}\right).$$

5.1. One dimensional case. The computational domain is $(0, 1)$. For example (1) and example (2), periodic boundary conditions are applied for ρ , u , χ and μ . For example (3) and example (4), mixed boundary conditions are $u|_{\partial\Omega=0}$, $\frac{\partial\chi}{\partial x}|_{\partial\Omega}=0$ and $\frac{\partial\mu}{\partial x}|_{\partial\Omega}=0$. For both these boundary condition cases, asymptotic stability results are presented in [9].

(1) The initial data that lie in the unstable region A_{unstable} with

$$(\rho_0, u_0, \chi_0)^T = \left(0.9, 0.5e^{-4(x-G_x)^2}, 0.4 + 0.4\sin(2\pi(x-1))\right)^T.$$

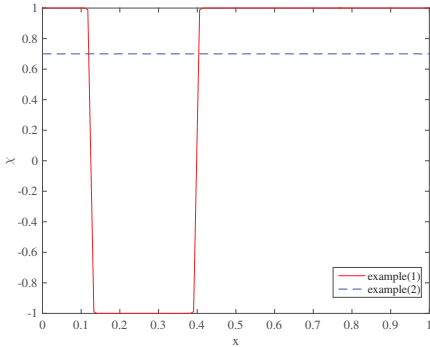
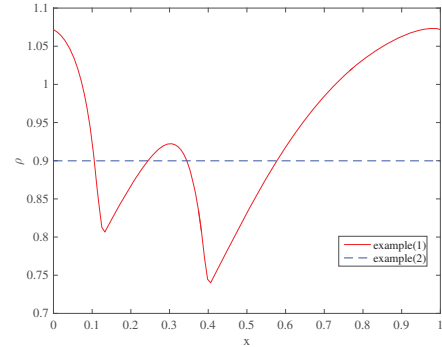
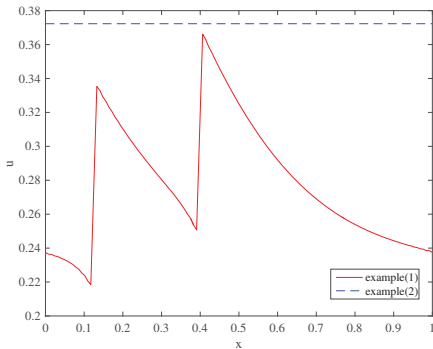
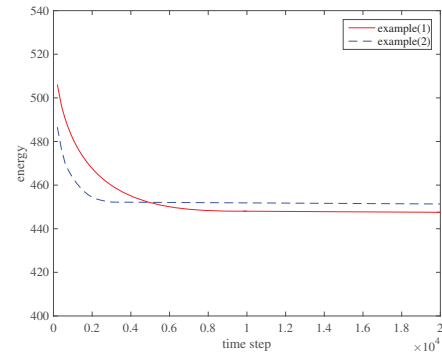
FIG. 5.1. Plot of χ at time $T = 100$.FIG. 5.2. Plot of ρ at time $T = 100$.FIG. 5.3. Plot of u at time $T = 100$.

FIG. 5.4. Behavior of energy as a function of time.

(2) The initial data that lie in the stable region A_{stable} with

$$(\rho_0, u_0, \chi_0)^T = \left(0.9, 0.5e^{-4(x-G_x)^2}, 0.7 + 0.3\sin(2\pi(x-1)) \right)^T.$$

Figures 5.1–5.3 show the behaviours of χ , ρ and u at $T = 100$. It is obvious to see that when the average of initial data of χ is in A_{unstable} (example (1)), the separation of phase is obtained in steady state. When the average of initial data of χ is in A_{stable} (example (2)), the solution remains in stable region. In both these examples, the discrete energy defined in (5.2) decays in time which is shown in Figure 5.4. The difference between example (1) and example (2) is the initial data of χ_0 , which is the essential reason that leads to the different asymptotic behaviors. The numerical simulations verify Theorem 4.1.

(3) The initial data is taken as

$$(\rho_0, u_0, \chi_0)^T = \left(0.9 + 0.001\cos(2\pi(x-1)), 0.5e^{-50(x-G_x)^2}, \tanh\left(\frac{x-G_x}{0.1\sqrt{5.0}}\right) \right)^T.$$

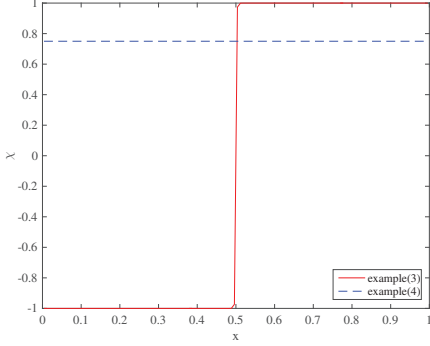
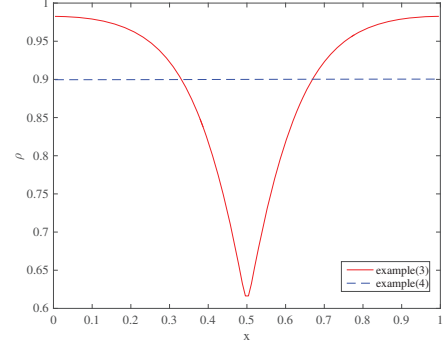
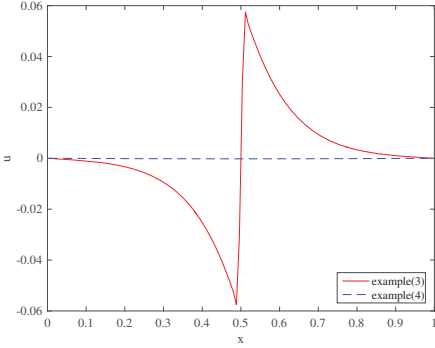
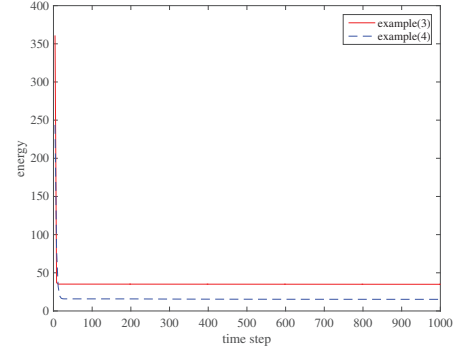
FIG. 5.5. Plot of χ at time $T=100$.FIG. 5.6. Plot of ρ at time $T=100$.FIG. 5.7. Plot of u at time $T=100$.

FIG. 5.8. Behavior of energy as a function of time.

(4) The initial data is taken as

$$(\rho_0, u_0, \chi_0)^T = \left(0.9 + 0.001 \cos(2\pi(x-1)), 0.5 e^{-50(x-G_x)^2}, \frac{\tanh\left(\frac{x-G_x}{0.1\sqrt{5.0}}\right)}{5.0} + 0.75 \right)^T,$$

where $G_x = 0.5$. Figures 5.5–5.7 show the behaviours of χ , ρ and u at $T=100$. The phase separation is observed when initial average concentration difference χ lies in unstable region (example (3)), in contrast, there is no phase separation when initial average concentration difference χ lies in stable region (example (4)). Discrete energy defined in (5.2) decays rapidly in time which is shown in Figure 5.8. The difference between example (3) and example (4) is the initial data of χ_0 . The numerical results are consistent with theoretical results in Theorem 4.1. We present another two examples related to compressible flows with $\epsilon=10^{-3}$, $\eta=10^{-8}$, $\nu=10^{-4}$ and $\gamma=1.4$.

(5) The initial data is taken as

$$(\rho_0, u_0, \chi_0)^T = (1.0, 0.0, 0.3 + 0.3 \sin(2\pi(x-1)))^T, \quad 0 \geq x < 0.5,$$

$$(\rho_0, u_0, \chi_0)^T = (0.125, 0.0, 0.3 + 0.3 \sin(2\pi(x-1)))^T, \quad 0.5 \geq x \leq 1.0.$$

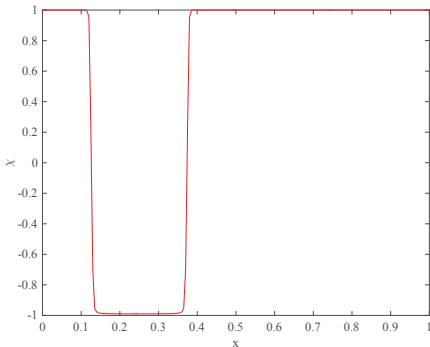
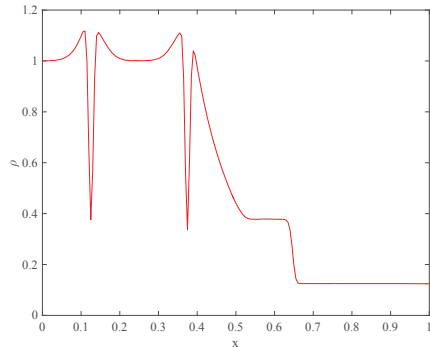
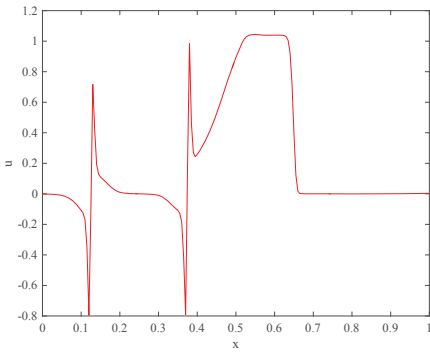
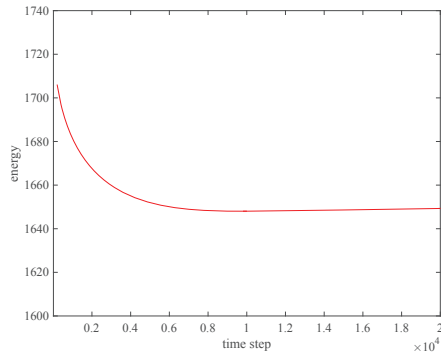
FIG. 5.9. Plot of χ at time $T=0.16$.FIG. 5.10. Plot of ρ at time $T=0.16$.FIG. 5.11. Plot of u at time $T=0.16$.

FIG. 5.12. Behavior of energy as a function of time.

(6) The initial data is taken as

$$\begin{aligned} (\rho_0, u_0, \chi_0)^T &= (0.311, 0.698, 0.3 + 0.3 \sin(2\pi(x-1)))^T, \quad 0 \geq x < 0.5, \\ (\rho_0, u_0, \chi_0)^T &= (0.5, 0.0, 0.3 + 0.3 \sin(2\pi(x-1)))^T, \quad 0.5 \geq x \leq 1.0, \end{aligned}$$

where $G_x = 0.5$. Figures 5.9–5.11 show the behaviours of χ , ρ and u at $T = 0.16$ when initial data is taken as (5). Discrete energy decays in time which is shown in Figure 5.12. Figures 5.13–5.15 show the behaviours of χ , ρ and u at $T = 0.17$ when initial data is taken as (6). Discrete energy decays in time which is shown in Figure 5.16. Both cases show that for low viscosity cases, phase separation will greatly affect the evolution of density and velocity. This scheme can be capable of simulating low viscosity cases which are like Euler equations but with additional phase variable.

5.2. Accuracy check. To check the accuracy of our scheme, we simulate example (1) and example (3) in 1-D case with different mesh sizes. The grids used are $J = 64, 128, 256, 512, 1024$, and the time step is taken to satisfy the condition in Theorem

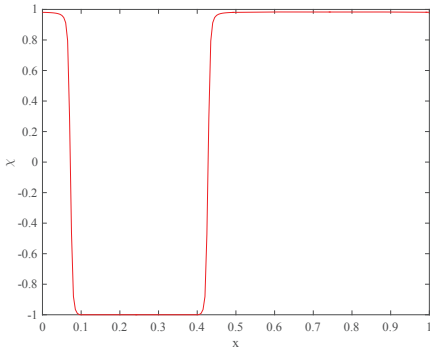
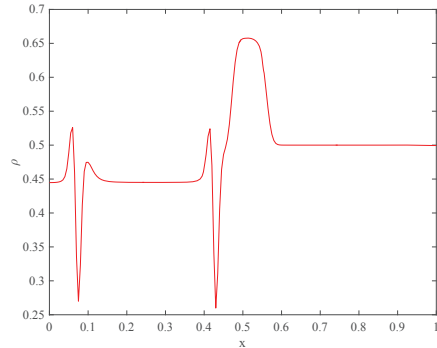
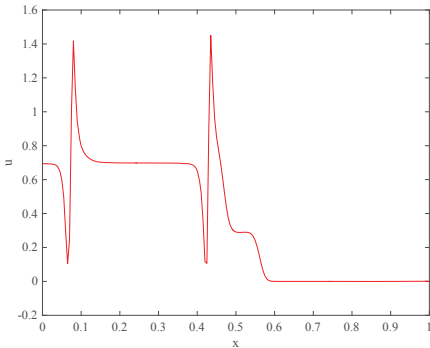
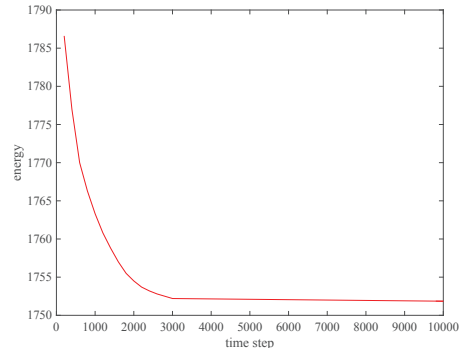
FIG. 5.13. Plot of χ at time $T=0.17$.FIG. 5.14. Plot of ρ at time $T=0.17$.FIG. 5.15. Plot of u at time $T=0.17$.

FIG. 5.16. Behavior of energy as a function of time.

N	$E_J(\chi)$	Rate	$E_J(u)$	Rate	$E_J(\rho)$	Rate
(64)-(128)	1.85e-3		3.58e-4		4.34e-4	
(128)-(256)	4.52e-4	2.03	8.86e-5	2.01	1.05e-4	2.04
(256)-(512)	1.12e-4	2.01	2.19e-5	2.01	2.61e-5	2.00
(512)-(1024)	2.81e-5	1.99	5.50e-6	1.99	6.62e-6	1.98

TABLE 5.1. L_2 norm of the error (5.3) and convergence rate for phase χ , velocity u and density ρ at time $T=1.0$ with different grids for example (1).

N	$E_J(\chi)$	Rate	$E_J(u)$	Rate	$E_J(\rho)$	Rate
(64)-(128)	8.85e-3		8.86e-4		9.43e-4	
(128)-(256)	2.15e-3	2.04	2.16e-4	2.04	2.23e-4	2.08
(256)-(512)	5.37e-4	2.00	5.25e-5	2.04	5.47e-5	2.03
(512)-(1024)	1.37e-4	1.97	1.33e-5	1.98	1.38e-5	1.99

TABLE 5.2. L_2 norm of the error (5.3) and convergence rate for phase χ , velocity u and density ρ at time $T=1.0$ with different grids for example (3).

time step	$E_{\Delta t}(\chi)$	Rate	$E_{\Delta t}(u)$	Rate	$E_{\Delta t}(\rho)$	Rate
$(\Delta t)-(\frac{\Delta t}{2})$	4.43e-2		7.65e-3		8.12e-3	
$(\frac{\Delta t}{2})-(\frac{\Delta t}{4})$	1.09e-2	2.02	1.91e-3	2.00	2.01e-3	2.01
$(\frac{\Delta t}{4})-(\frac{\Delta t}{8})$	2.72e-3	2.00	4.82e-4	1.99	5.08e-4	1.98

TABLE 5.3. L_2 norm of the error (5.4) and convergence rate for phase χ , velocity u and density ρ at time $T=1.0$ with different time steps with $h=1/512$ for example (1).

time step	$E_{\Delta t}(\chi)$	Rate	$E_{\Delta t}(u)$	Rate	$E_{\Delta t}(\rho)$	Rate
$(\Delta t)-(\frac{\Delta t}{2})$	9.72e-2		1.23e-2		3.32e-2	
$(\frac{\Delta t}{2})-(\frac{\Delta t}{4})$	2.46e-2	1.99	3.08e-3	2.00	8.26e-3	2.01
$(\frac{\Delta t}{4})-(\frac{\Delta t}{8})$	6.23e-3	1.98	7.79e-4	1.98	2.09e-3	1.98

TABLE 5.4. L_2 norm of the error (5.4) and convergence rate for phase χ , velocity u and density ρ at time $T=1.0$ with different time steps with $h=1/512$ for example (3).

4.1. The L_2 norm of the error is calculated by

$$E_J(\cdot) = \left[\sum_{i=1}^J [(\cdot)_J(i) - (\cdot)_{2J}(2i)]^2 h \right]^{1/2}, \quad (5.3)$$

where $(\cdot)_J$ is calculated for three different variables ρ, u, χ in the following tables and $h=1/J$. The convergence rate is calculated by $\log_2(E_J/E_{2J})$. The results in Table 5.1 and Table 5.2 show second-order accuracy for all quantities χ, u and ρ . In order to verify the rate for time, we calculate the L_2 norm of the error for $h=1/512$,

$$E_{\Delta t}(\cdot) = \left[\sum_{i=1}^J [(\cdot)_{\Delta t}(i) - (\cdot)_{\frac{\Delta t}{2}}(i)]^2 h \right]^{1/2}. \quad (5.4)$$

The convergence rate is calculated by $\log_2(E_{\Delta t}/E_{\frac{\Delta t}{2}})$. Table 5.3 and Table 5.4 show second-order accuracy in time.

5.3. Two dimensional case. For the two dimensional case, the computational domain is $(0,1) \times (0,1)$ and the viscosity coefficient λ in (2.38) is $\lambda=1.0$ and parameters ϵ, η, ν are chosen as in (5.1). Periodic boundary conditions are applied for ρ, u, v, χ and μ both in x and y direction. The energy has a similar formulation as in the one dimensional case:

$$Eng_{2D} = \|(\sqrt{a} + \sqrt{b})\mathbf{u}^n\|^2 + \|\mathbf{v}^n\|^2 + \|\mathbf{w}^n\|^2 + \frac{\epsilon}{2h^2} \sum_{i,j=1}^J (\nabla \chi_{i,j}^n)^2 + \frac{1}{\epsilon} \sum_{i,j=1}^J \rho_{i,j}^n f_{i,j}^n, \quad (5.5)$$

where a and b are defined in Section 2.2.

(1) The initial data is taken as

$$(\rho_0, u_0, v_0, \chi_0)^T = \left(1.6, 0.5e^{-4((x-G_x)^2 + (y-G_y)^2)}, 0.5e^{-4((x-G_x)^2 + (y-G_y)^2)}, \tanh \left(\frac{-\sqrt{(x-G_x)^2 + (y-G_y)^2} + 0.25}{0.05} \right) \right)^T,$$

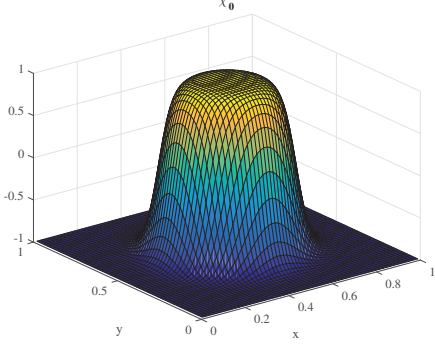
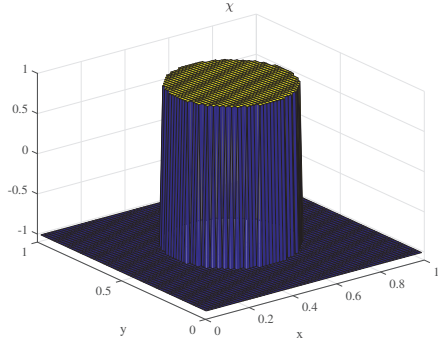
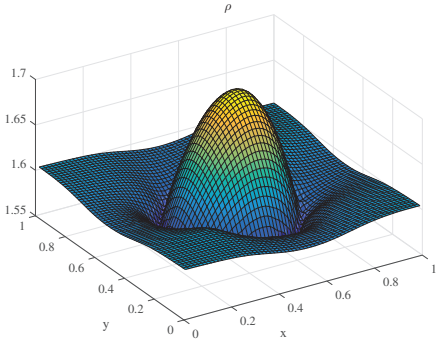
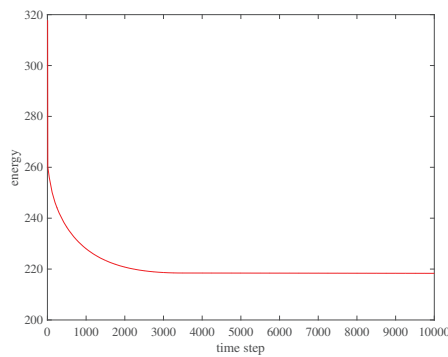
FIG. 5.17. Surface plot of χ at time $T=0$.FIG. 5.18. Surface plot of χ at time $T=100$.FIG. 5.19. Surface plot of ρ at time $T=100$.

FIG. 5.20. Behavior of energy as a function of time.

the initial average concentration difference lies in the unstable region A_{unstable} . Figures 5.17–5.19 show the separation of phase, and Figure 5.20 shows that energy is decaying, which is similar to the one dimensional case.

(2) The initial data is taken as

$$(\rho_0, u_0, v_0, \chi_0)^T = \left(1.6, 0.5e^{-4((x-G_x)^2 + (y-G_y)^2)}, 0.5e^{-4((x-G_x)^2 + (y-G_y)^2)}, \frac{1}{5.0} \tanh \left(\frac{-\sqrt{(x-G_x)^2 + (y-G_y)^2} + 0.25}{0.05} \right) + 0.8 \right)^T,$$

the initial average concentration difference lies in the stable region A_{stable} , where $G_x = 0.5, G_y = 0.5$. Figures 5.21–5.23 show the solutions go to a stable steady state, and Figure 5.24 shows that energy is still decaying, which is similar to the one dimensional case.

6. Concluding remarks

We present a relaxation scheme coupled with a stabilized method to solve compressible Navier-Stokes-Cahn-Hilliard system. The scheme is shown to have energy-decaying property which ensures stability of the scheme. Numerical results show that the aver-

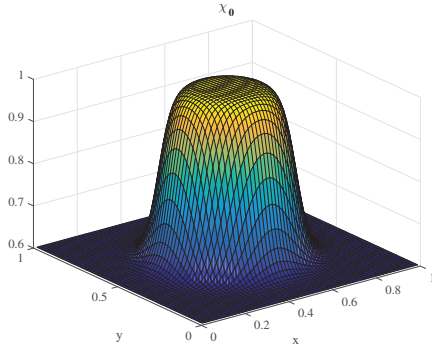
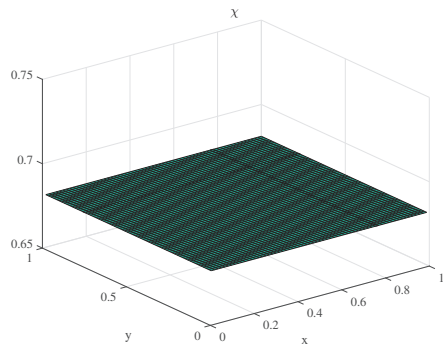
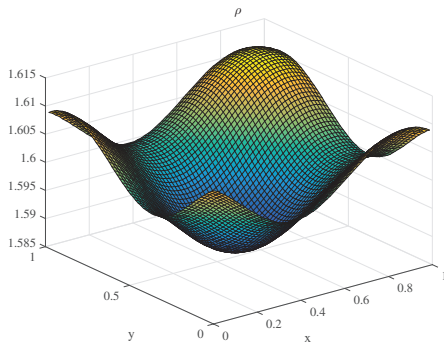
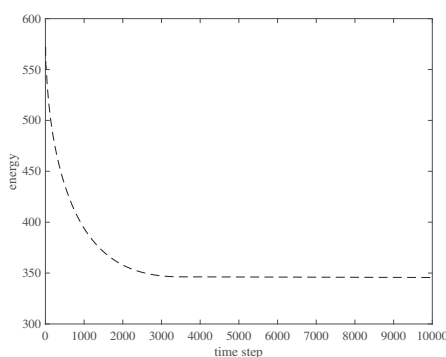
FIG. 5.21. Surface plot of χ at time $T=0$.FIG. 5.22. Surface plot of χ at time $T=100$.FIG. 5.23. Surface plot of ρ at time $T=100$.

FIG. 5.24. Behavior of energy as a function of time.

age concentration difference for the two components of the initial state determines the long-time behavior of the diffusive interface for the two-phase flow, which verifies the asymptotic stability in [9] numerically. In the future, we will extend our method to the situation for large viscosity ratio. We will also work on the gas-liquid phase transition represented by a diffuse interface model with van der Waals equation of state, and is composed of the compressible Navier-Stokes system and a modified Allen-Cahn equation.

Acknowledgments. This research is supported in part by National Key R & D Program of China (2018YFC0830300) and NSFC (No. 11201322, No. 11671027, No. 11971020).

REFERENCES

- [1] J. Lowengrub and L. Truskinovsky, *Quasi-incompressible Cahn-Hilliard fluids and topological transitions*, Proc. Roy. Soc. A Math. Phys. Eng. Sci., **454**:2617–2654, 1998. 1, 2
- [2] H. Abels and E. Feireisl, *On a diffuse interface model for a two-phase flow of compressible viscous fluids*, Indiana Univ. Math. J., **57**(2):659–698, 2008. 1
- [3] D.M. Anderson, G.B. McFadden, and A.A. Wheeler, *Diffuse-interface methods in fluid mechanics*, Annu. Rev. Fluid Mech., **30**:139–165, 1998. 1

- [4] M. Heida, J. Málek, and K.R. Rajagopal, *On the development and generalizations of Cahn-Hilliard equation within a thermodynamic framework*, Z. Angew. Math. Phys., **63**(1):145–169, 2012. 1
- [5] M. Kotschote, *Mixing rules and the Navier-Stokes-Cahn-Hilliard equations for compressible heat-conductive fluids*, Bull. Brazilian Math. Soc., **47**(2):457–471, 2016. 1, 2
- [6] P.L. Lions, *Mathematical Topics in Fluid Mechanics. Volume 2: Compressible Models*, Oxford University Press, New York, 2, 1998. 1
- [7] M. Kotschote and R. Zacher, *Strong solutions in the dynamical theory of compressible fluid mixtures*, Math. Models Meth. Appl. Sci., **25**(07):1217–1256, 2015. 1
- [8] S. Ding and Y. Li, *Well-posedness for 1D compressible Navier-Stokes/Cahn-Hilliard system*, preprint, 2012. 1
- [9] Y. Chen, Q. He, M. Mei, and X. Shi, *Asymptotic stability of solutions for 1-D compressible Navier-Stokes-Cahn-Hilliard system*, J. Math. Anal. Appl., **467**(1):185–206, 2018. 1, 4.2, 5.1, 6
- [10] N. Alikakos, P.W. Bates, and G. Fusco, *Slow motion for the Cahn-Hilliard equation in one space dimension*, J. Diff. Eqs., **90**:81–135, 1991. 1, 2
- [11] P.W. Bates and P.C. Fife, *The dynamics of nucleation for the Cahn-Hilliard equation*, SIAM J. Appl. Math., **53**:990–1008, 1993. 1
- [12] P.W. Bates and J. Xun, *Metastable patterns for the Cahn-Hilliard equation. II. Layer dynamics and slow invariant manifold*, J. Diff. Eqs., **117**:165–216, 1995. 1
- [13] L. Bronsard and R. Kohn, *On the slowness of phase boundary motion in one space dimension*, Comm. Pure Appl. Math., **43**:983–998, 1990. 1
- [14] J. Carr, M. Gurtin, and M. Slemrod, *Structured phase transition on a finite interval*, Arch. Ration. Mech. Anal., **86**:317–351, 1984. 1
- [15] R.L. Pego, *Front migration in the nonlinear Cahn-Hilliard equation*, Proc. Roy. Soc. London Ser. A, **422**:261–278, 1989. 1
- [16] M. Gao and X.P. Wang, *A gradient stable scheme for a phase field model for the moving contact line problem*, J. Comput. Phys., **231**:1372–1386, 2012. 1
- [17] Q. He, R. Glowinski, and X.P. Wang, *A least-squares/finite element method for the numerical solution of the Navier-Stokes-Cahn-Hilliard system modeling the motion of the contact line*, J. Comput. Phys., **230**:4991–5009, 2011. 1
- [18] R.H. Guo and Y. Xu, *Efficient, accurate and energy stable discontinuous Galerkin methods for phase field models of two-phase incompressible flows*, Commun. Comput. Phys., **26**(4):1224–1248, 2019. 1
- [19] S. Jin and Z.P. Xin, *The relaxation schemes for systems of hyperbolic conservation laws in arbitrary space dimensions*, Comm. Pure Appl. Math., **48**:235–276, 1995. 1, 2, 2.1, 2.1, 2.2, 2.2
- [20] J. Shen and X.F. Yang, *Numerical approximations of Allen-Cahn and Cahn-Hilliard equations*, Discrete Contin. Dyn. Syst., **28**(4):1669–1691, 2010. 1, 2.1, 4.1, 4.1
- [21] A. Chalabi, *Convergence of relaxation scheme for hyperbolic conservation laws with stiff source terms*, Math. Comput., **68**(227):955–970, 1999. 2
- [22] A. Chalabi and Y. Qiu, *Relaxation schemes for hyperbolic conservation laws with stiff source terms: application to reacting Euler equations*, J. Sci. Comput., **15**(4):395–416, 2000. 2
- [23] C. Lattanzio and D. Serre, *Convergence of a relaxation scheme for hyperbolic systems of conservation laws*, Numer. Math., **88**(1):121–134, 2001. 2
- [24] Q. He, C. Liu, and X. Shi, *Numerical study of phase transition in van der Waals fluid*, Discrete Contin. Dyn. Syst. B, **23**(10):4519–4540, 2018. 2
- [25] S. Jin, *Runge-Kutta methods for hyperbolic conservation laws with stiff relaxation terms*, J. Comput. Phys., **122**(1):51–67, 1995. 2.1
- [26] P.R. Sweby, *High resolution schemes using flux limiters for hyperbolic conservation laws*, SIAM J. Numer. Anal., **21**:995–1011, 1984. 2.1